J Mater Sci: Mater Electron

Development of geopolymer composites for EMI shielding from steel industry waste

Rahul Sharma[1], William Clower[1], Sudhir Amritphale[2], Shaurav Alam[2], John Matthews[2], and Adarsh D. Radadia[1,*]

[1] Institute for Micromanufacturing, Louisiana Tech University, Ruston, LA 71272, USA
[2] Trenchless Technology Center, Louisiana Tech University, Ruston, LA 71272, USA

Received: 12 September 2021
Accepted: 27 December 2021

ABSTRACT

In this study waste from steel industries, namely, mill scale, red dust, and iron ore fines have been used as additives in geopolymer matrix for imparting EMI shielding properties in the developed composite material. geopolymer is inherently more conductive in comparison to conventional cement matrix and helps to achieve better EMI shielding. For a 30-mm geopolymer sample the EMI SE was found to be up to 9 dB in the frequency range 0.1 to 1.5 GHz. The EMI SE values for steel industry waste material, namely, mill scale, red dust, and iron ore fine were found to be 24 dB, 12 dB, and 10 dB, respectively. The addition of iron ore fine had the least change in EMI SE value of geopolymer, while the addition of mill scale had the most change in EMI SE value of geopolymer. The addition of 10 wt% SS fiber in geopolymer control sample resulted in enhanced EMI SE value 28–69 dB. Further as little as 2 wt% of steel fiber along with mill scale helped enhance EMI SE value up to 22–67 dB. As electrical conductivity of geopolymer is low, the magnetic properties like saturation magnetization helps in improving the EMI shielding of the composites. Mill scale geopolymer had the highest saturation magnetization of 22.165 emu/g, followed by red dust geopolymer 10.69 emu/g and iron ore fine geopolymer (1.76 emu/g). The control sample had the least magnetization 1.34 emu/g and the least EMI shielding. Impedance spectroscopy and equivalent circuit modeling show that electrical conductivity alone was not responsible for the observed change in EMI SE upon addition of steel industry waste and SS fiber. The magnetic properties of the geopolymer composites were responsible for the EMI shielding in the geopolymer composites. Further, this study clearly shows that geopolymer-based EMI shielding composite material can be used as a building material due to adequate compressive strength (up to 30 MPa) of the developed material.

Address correspondence to E-mail: radadia@latech.edu

https://doi.org/10.1007/s10854-021-07674-9
Published online: 03 February 2022

1 Introduction

The increased use of electronic devices in our daily lives has led to increased health problems among the public, which could be worsened with the arrival of Internet of Things (IoT) [1] and other upcoming 5G technologies. This could lead to increased exposure to EM pollution [2], which may adversely affect human health. Also, at risk are public infrastructure like airports, hospitals, and other buildings housing-sensitive electronic equipment which may be susceptible to EM interference and cyber security threats [3]. Exposure of children and pregnant women to EM Waves is also particularly very harmful [4]. With the widespread use of mobile phones, base stations, radar systems, and electronics in our daily life it is difficult to live a modern life without the side effects of EM waves. But it is possible to mitigate the effects of EMI pollution by making materials which absorb/reflect EM waves by adding fillers in already existing materials to enhance its EMI shielding properties. So far most of the EMI shielding work has been done in the X-band as most of the need comes from this section to provide shielding to aircraft electronics, satellites, and other equipment operating in the X-Band. To provide EMI shielding to house-sensitive electronics and other equipment we currently use Cu-protect® which is an alloy of Cu. It can provide very good EMI Shielding (60–80 dB) from 0.1 to 4 GHz [5]. It is very expensive to provide EMI shielding with this material and it is not suitable for large construction projects. It is commercially known as Cu-protect® and is currently the state-of-the-art in EMI shielding. However, with the growing demand for EMI shielding there is a need to make a building construction material which can provide EMI shielding at an affordable price. Many research groups are working in this regard to make EMI shielding building construction materials. Both ordinary Portland cement (OPC) and geopolymer are being used as a base to make EMI shielding concrete, which can be used for housing project where EMI shielding is needed. Novias et al. have shown that pyrolyzed cork geopolymer composite can be used as EMI shielding material in the X-band (8–12 GHz) having total shielding effectiveness values from − 13.8 to − 15.9 dB and the carbon content from recycled cork was only (2.5–3.75 wt%), comparatively lower than other reported in literature [6]. Jung et al. has demonstrated EMI shielding cement based on CNT. The SE values reported were 20–25 dB in the frequency range of 30 MHz to 1.5 GHz for 3-mm-thick samples tested according to ASTM-D4395-18 standard [7]. Dhawan et al. prepared Multi-walled CNT/OPC composites for EMI shielding in the X-band. The results showed that they are effective for EMI shielding in the X-band, i.e., (8–12 GHz). The inclusion of 15 wt% of multi-walled CNT in the OPC matrix resulted in an EMI shielding effectiveness of 27 dB, in the X-band [8]. Further material characterizations like SEM, XRD, and X-ray photoelectron spectroscopy were performed to determine the dominant mechanism of shielding in the composites. The dominant mechanism after materials characterization was found to be absorption. Han et al. used nickel fibers in cementitious composite to increase the electrical conductivity and EMI shielding effectiveness. The electrical conductivity upon addition of nickel fiber was determined to be 2.65×10^{-3} S/cm. The EMI shielding effectiveness at 9 vol.% of nickel fiber powder was found to be 19.85 to 24.48 dB in the frequency range of 1 to 1500 MHz [9]. Guo et al. reported the use of stainless steel furnace dust as an admixture for preparing EMI shielding cementitious composites, the EMI shielding effectiveness for a 45 mass % of stainless steel furnace dust was 6–9 dB in the frequency range of 500 MHz to 1.5 GHz, and the method used for measuring EMI shielding effectiveness was coaxial cable method [10]. Scrap tires wire was used by Yang et al. to prepare EMI shielding cementitious composites containing FeCuNbSiB amorphous alloy. Coaxial planar spectrum analyzer method was used to determine the EMI shielding effectiveness of the cementitious composites. The EMI SE at 1.5 GHz was 14.1 dB and the scrap wire content was 1.3 vol.% in cement paste [11]. Tuan et al. have shown that a high-performance EMI shielding concrete is possible in a wide frequency range 10 kHz to 18 GHz [12]. The research by Tuan et al. has shown that EMI shielding concrete for construction purposes is very much possible due to successful commercialization of EMI shielding concrete. The spin-off Conductive Concrete Technologies from Tuan et al. has shown that EMI shielding concrete is very much possible and can be implemented in large-scale construction projects. In this regard our research group is trying to implement EMI shielding concrete based on steel industry waste, which can be used in large

construction projects. Also, the matrix selected for this study was geopolymer which has better engineering properties than OPC [13]. The wide availability of our raw material makes our concrete more sustainable and cost effective than OPC concrete. If large construction projects are to be implemented with EMI shielding properties than Cu-protect®-based EMI shielding will not offer a viable solution. Most of the EMI shielding is based on expensive metallic alloys, conductive paints, polymers, etc. which are very expensive to use and not feasible for use as building construction material. In this work, a 2-part geopolymer system was used for making EMI shielding composites; it is also possible to make similar composites with a 1-part geopolymer system which overcomes all the limitations and handling issues from 2-part geopolymer system. Thus, we present an EMI shielding concrete based on geopolymer and fillers from the steel industry waste which can be used for EMI shielding in large-scale engineering construction projects. The figure of merit in EMI shielding is the Shielding Effectiveness, measured in decibel (dB). The Shielding effectiveness can be defined as a parameter that measures how well a material can prevent the propagation of EM wave of a particular frequency through it. When an EM wave of a particular frequency falls on the surface of the material some of it is reflected, some of it is transmitted and some gets absorbed by the material. The total Shielding effectiveness is the sum of the three.

The total SE is given by

$$SE_T(dB) = 10log\frac{P_I}{P_T}, \quad (1)$$

Here, P_I is the power of the incident EM wave and P_T is the power of the transmitted EM wave. The USA is one of the largest steel producers in the world and generates a lot of steel waste. Some of the common steel industry wastes are electric arc furnace slag, ladle furnace slag, mill scale, red dust, and iron ore fine. This industry waste has potential as fillers to make EMI shielding building material. One major concern for construction material is that it should be abundant and cheaply available. These steel industry waste fulfill these requirements. Mill scale is formed during the heating/re-heating and cooling of steel bars. Mill scale is the flaky surface consisting of iron oxides. Mill scale has been used as a filler to make a ceramic-based EMI shielding material [14]. Recently mill scale has been used as a filler in cementitious composite for EMI shielding applications [15]. However, to the best of our knowledge no work has been reported on geopolymer mill scale composites for EMI shielding applications. Red dust or steel dust has been used for making cementitious composites for EMI shielding application [16], but no such work has been reported in geopolymer composites. Iron ore fine has never been used as an admixture for EMI shielding in either cement or geopolymer matrix and is available in large quantities.

2 Materials and methods

Sodium hydroxide (16 Molar) in pellet form was purchased from Fisher Scientific (Waltham, MA, USA). Different type of wastes from steel industry, namely, mill scale, iron ore fine, and red dust were supplied by Phoenix Services (Portage, IN, USA). The steel waste was generated at Arcelor Mittal steel plant (Burns Harbor, IN, USA). Mill scale as received from plant was passed through a sieve to ensure a particle size less than 425 microns and removal of aggregates. Red dust and iron ore fine were passed through a larger sieve; the particle size of red dust and iron ore fine was between 425 and 825 microns. Sodium silicate (45% w/w solution) was purchased from Mini-Sciences Inc. (Clifton, NJ, USA). Class F Fly Ash was used as received from Martin Lake Power Plant (Tatum, TX, USA) and Boral Resources (flyash.com).

2.1 Synthesis of geopolymer composites

geopolymer samples without EMI shielding additives were prepared by mixing fly ash (2120 g) and sodium hydroxide solution (264 g) in 12:1 (w:w) ratio. After stirring initially by hand, a stand mixer was used for thorough mixing for 5 min at 50 rpm. Then sodium meta silicate (340 gm) was added to the mixture and stirred till we achieved a good workability. For geopolymer composites with EMI shielding additives homogenization of fly ash, sodium hydroxide, and sodium metasilicate as above, followed by addition of the metal additive to the slurry and stirring for another 5 min. The mixture was poured into circular molds of desired size. For EMI SE testing according to the ASTM-D-4935, three molds were used—one was a 133 mm diameter and

30 mm height, second was annular ring with an inner and an outer diameter of 76 mm and 133 mm, respectively. The molds were cured in the oven for 24 h at 67 °C. Thermal stress in the samples was relieved by cooling samples over an hour from over to room temperature. Demolded samples were used only after cleaning them with a dry cloth and conditioning them for 2 h at ambient conditions.

2.2 Materials characterization

The surface morphology of raw materials was evaluated by field emission scanning electron microscopy (FE-SEM, Hitachi S4800). The samples were mounted in the form of dry powder on a double-sided carbon tape and care was taken to remove loose debris with gentle knocking and pressurized air flow. Since some of the samples tested here were inherently magnetic the imaging was challenging as the magnetic particles could deflect and damage the column of the SEM. The surface morphology plays a very important role in EMI shielding and will be discussed further in the results and discussion section. The energy-dispersive X-ray spectrometer (EDAX) coupled with the FE-SEM provided the elemental analysis of the samples. X-ray diffraction (XRD) analysis to reveal mineralogical phases in the raw materials was obtained using a Bruker D-8 X-ray diffractometer equipped with a Cu-Kα radiation source (1.54060 Å). The X-ray diffraction intensity was recorded as a function of Bragg's 2θ in the angular range of 10°–85° optical.

2.3 Magnetic properties characterization, ASTM-D-4935 shielding effectiveness testing

The magnetic characterization of various geopolymer composites have been studied using a vibrating sample magnetometer, Digital Measurement Systems model 880A. Various geopolymer composites in powder form were placed in sample holder and subjected to a constant magnetic field, for evaluating the magnetic properties. The system consists of a 4″ walker magnet and a bipolar power supply. VSM head and lock in amplifier, microprocessor-based control system, HP plotter, and printer along with a temperature control system over a range of − 170 to 730 °C. The mass of the various geopolymer composites was measured before performing the experiment. The measurements were performed at ambient conditions (23 °C, ∼ 55–60%RH). The EMI SE measurements were taken using an EM2017A from Electro-metrics Corporation as shown in Fig. 1a, coupled with a vector network analyzer (4396-B Agilent Technologies) and an Agilent 85046A S-parameter test set, which provide to measure the transmission and reflection characteristics of two port devices in either direction. The SE was measured in decibel (dB) between 100 MHz and 1.5 GHz with 10 dB attenuator at the input and output ports. The measurements were performed at ambient conditions (20 °C, ∼ 40–50%RH).

3 Experimental results and discussion

3.1 Characterization of raw material and geopolymer composites

The SEM images in Fig. 2 show the microstructure of each raw material. The elemental composition according to EDS for each are given in Table S1 (Supplementary information) and their crystalline phases.

is identified by XRD as shown in Fig. 3. As shown in Fig. 2a, fly ash exhibits a spherical morphology with a particle size below 20 μm. The spherical morphology of the fly ash enhances the EMI shielding properties of the prepared sample and is one of the reasons we have selected raw materials having spherical morphology [17]. Table S1 shows that fly ash composed of sodium, calcium, silicon, iron, and aluminum majorly. Figure 3a shows that only silicon was present in the crystalline form (silica) [18]. The XRD results of fly ash indicate that nearly 70% material is in amorphous form. As shown in Fig. 2b, the SEM images of iron ore fine show fine crystalline granular morphology of irregular size and shape distribution. Table S1 shows the presence of aluminum and silicon in addition to iron. Figure 3b shows that iron is present in both the crystalline phases of goethite and hematite. The hydroxide content of goethite phase has been known to be responsible for observed agglomeration of both the crystalline phases [19]. As shown in Fig. 2c, the SEM images of mill scale show spherical granular morphology primarily composed of iron and oxygen, with some irregular granular particles.

Table S1 shows the presence of carbon, aluminum, and silicon in addition to iron oxide in mill scale. The

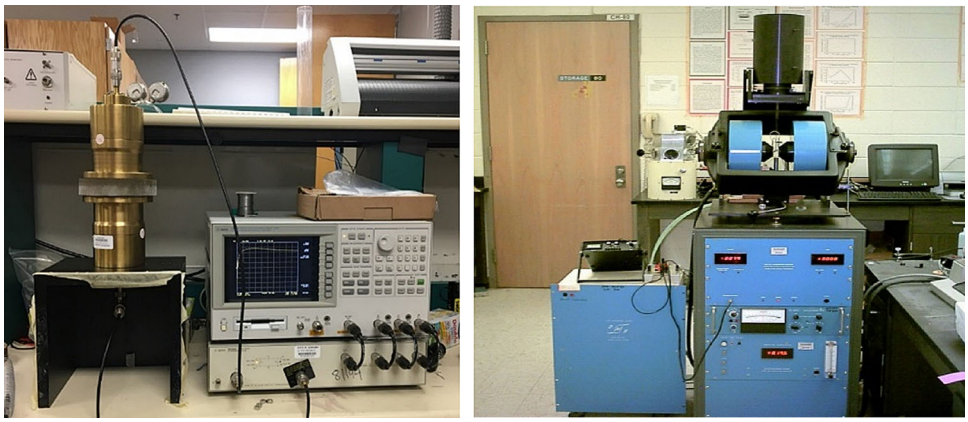

Fig. 1 **a** Set-up for shielding effectiveness measurement. **b** A vibrating sample magnetometer to measure the magnetic properties of the geopolymer composites

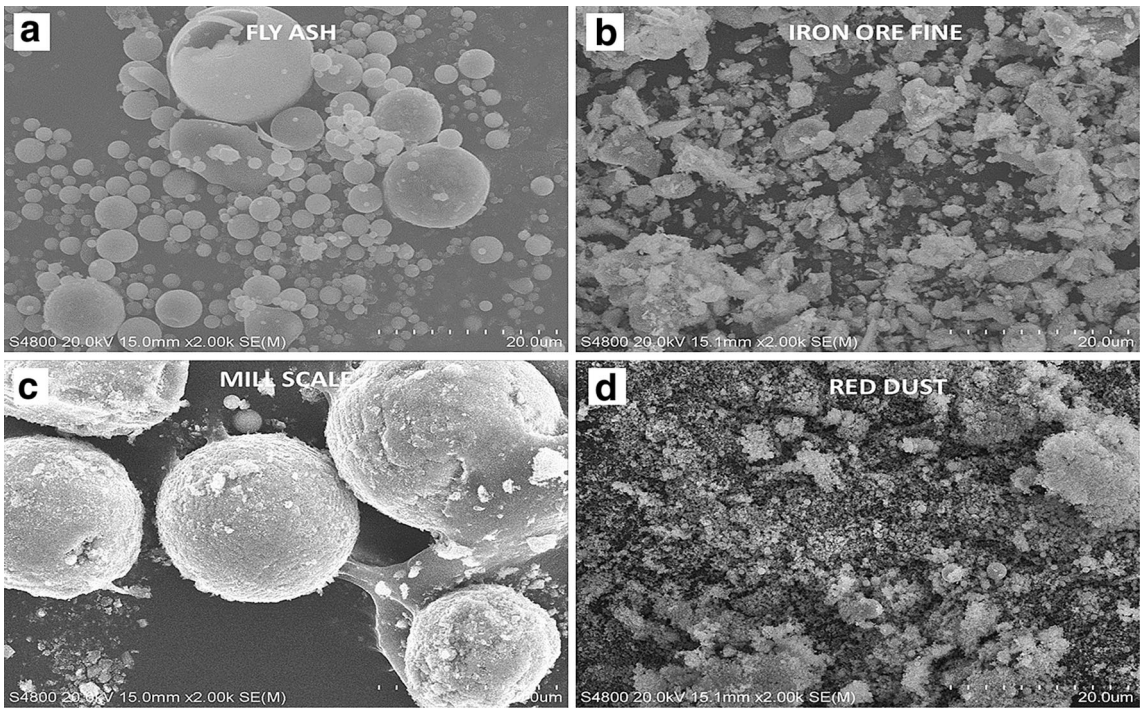

Fig. 2 Example of scanning electron microscopy images of **a** fly ash, **b** iron ore fine, **c** mill scale, and **d** red dust. Each image shows its imaging condition and relative scale in white

XRD of mill scale shown in Fig. 3c confirms the presence of iron as a mixture of magnetite and hematite phases of iron oxide; similar spectra have been shown by Carriazo et al. [20]. The SEM images of red dust in Fig. 2d show agglomeration of fine crystalline material. Table S1 shows that red dust is primarily composed of iron oxide and traces of carbon, calcium, and sodium. Figure 3d shows that iron oxide was majorly presented in red dust as a mixture of hematite and magnetite. Mill scale had the maximum iron content in it, followed by red dust and iron ore fines. But the iron is mainly present in oxide form. The spherical morphology of mill scale helps in enhancing the EMI SE of the geopolymer composites as it helps in multiple internal reflections. Multiple internal reflections of the EM wave within the geopolymer matrix helps in improving the shielding effectiveness of the sample. The presence of residual carbon in fly ash improves the shielding effectiveness on account of electrical conductivity of the residual carbon.

The X-ray diffraction pattern of fly ash shown in Fig. 3a shows the presence of quartz (SiO_2) mineral as major phase followed by crystalline phases of mullite

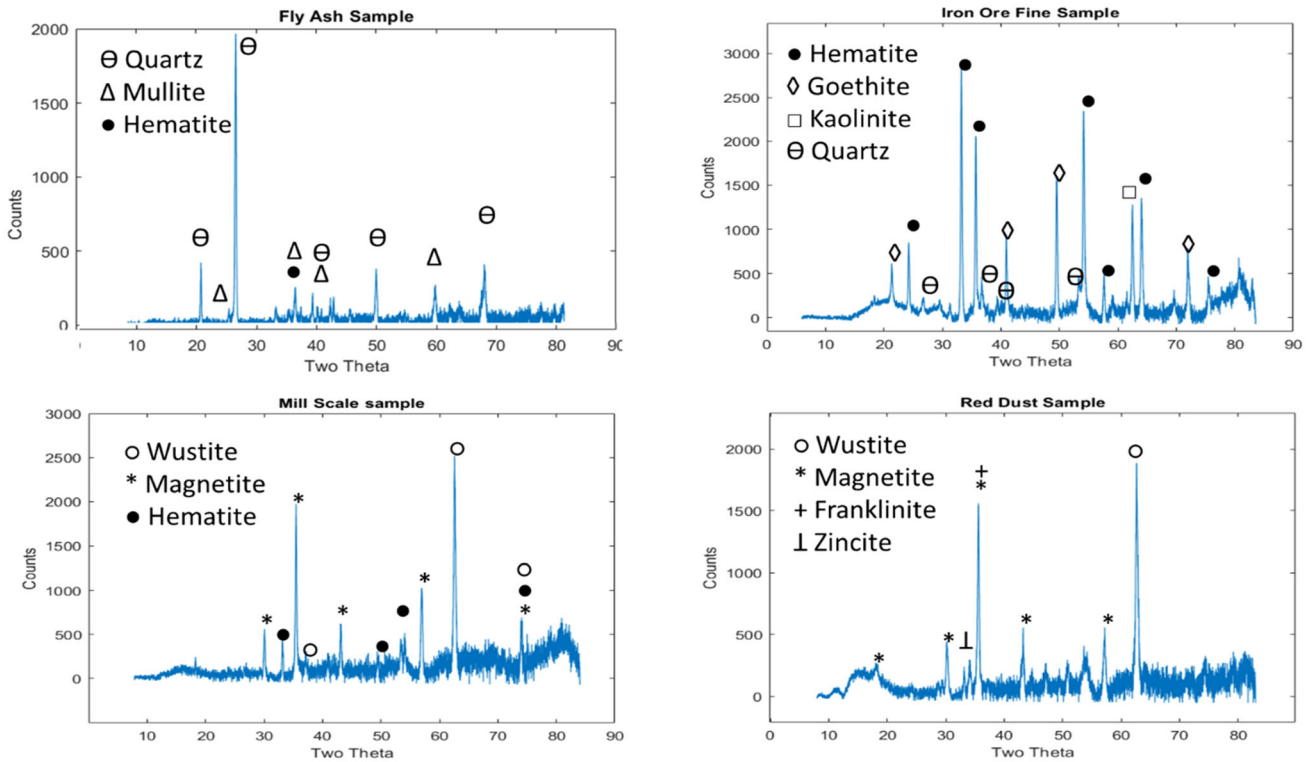

Fig. 3 XRD spectra for **a** fly ash, **b** iron ore fine, **c** mill scale, and **d** red dust. XRD signal is shown in blue. Blue lines show peak positions for identified crystal structure by the ICDD PDF-4 + library published in 2019. The spot size used in the XRD analysis is 0.5 mm

and hematite [21]. Recently Wang et al. have studied the use of SiCnw–SiO_2–NH_2 hybrids for dielectric properties and also high thermal conductivity characteristics [22]. Similarly, for iron ore fine the major phase consists of hematite and goethite along with minor phases of kaolinite clay and quartz mineral as shown in Fig. 3b and as reported in literature [23]. The XRD pattern of mill scale as seen in Fig. 3c shows the major phase as wustite with magnetite and hematite as minor phases [24]. Composites containing various form of iron oxides in combination with cobalt and copper nanocomposite have been studied for EMI application by Hou et al. and Liu et al. [25, 26]. The XRD of red dust also shows the presence of wustite and magnetite as major phase along with minor phases of franklinite and zincite (mineral form of ZnO) as evident from Fig. 3d. The observed peaks are in accordance with those reported in previous literature for red dust [27, 28]. Similarly, Guanglei Wu et al. have studied NiCo@C/ZnO composite for enhanced microwave absorption [29]. To determine the morphology of the finished geopolymer composites, field emission scanning electron microscopy was performed on the EMI shielding geopolymer composites. The first sample was control or the geopolymer composite without the use of any industrial fillers. The next geopolymer composite sample contained iron ore fines, followed by mill scale geopolymer composite and finally red dust geopolymer composite. The addition of various industrial waste materials to the geopolymer matrix can alter the electrical, magnetic, and electromagnetic interference shielding properties of the formed geopolymer matrix. Multiple internal reflections within the formed geopolymer matrix contribute to EMI shielding effectiveness. The presence of spherical particles within the geopolymer matrix will enhance the shielding effectiveness of the geopolymer sample, which can be analyzed by characterizing the morphology of the geopolymer composites after geopolymerization reaction has taken place. If non-spherical morphology is produced, then it might affect the EMI shielding properties of the formed geopolymer composites.

From Fig. 4, it can be observed that the geopolymer composite formed has flake-like morphology, which is not conducive to formation of effective EMI shielding composites. On the other hand, it can be

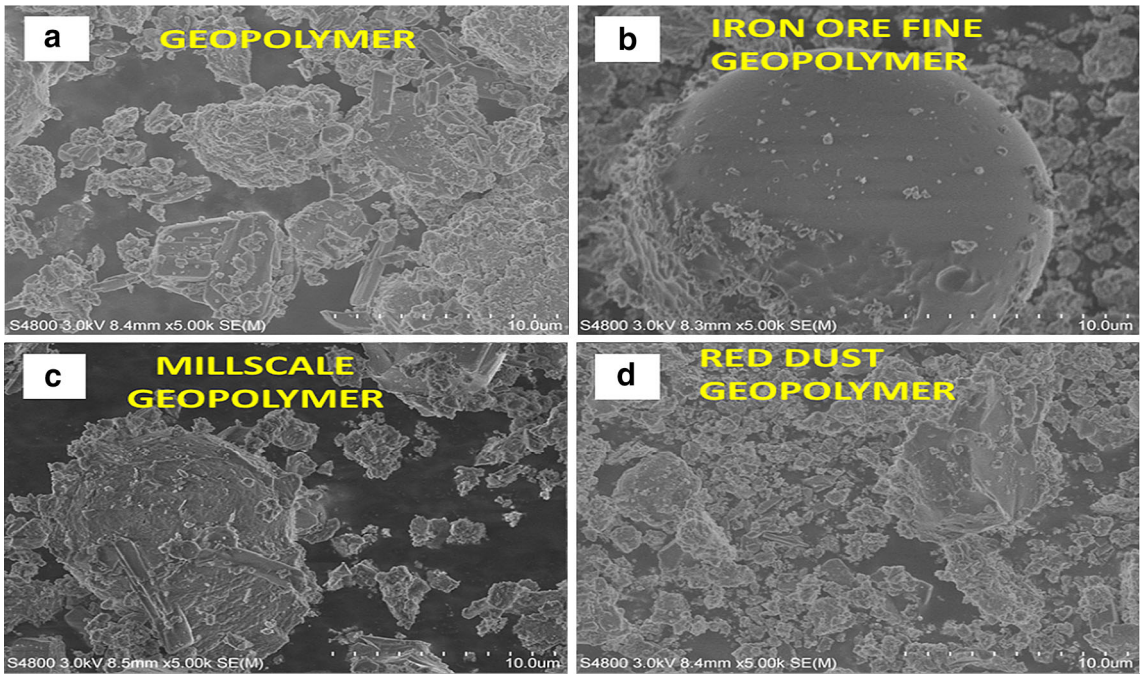

Fig. 4 Scanning electron microscopy images of the formed geopolymer composites **a** pure geopolymer, **b** iron ore fine geopolymer composite, **c** mill scale geopolymer composites, and **d** red dust geopolymer composites

observed that iron ore fines and mill scale geopolymer composites have a better EMI shielding performance than pure geopolymer due to presence of large number of interconnected zones and higher saturation magnetization values.

The XRD spectra for the mill scale geopolymer composite has hematite and magnetite as dominant phases, which were present from mill scale itself. The other dominant peaks are from quartz and mullite. The less dominant peaks are due to calcite and wustite as shown in Fig. 5.

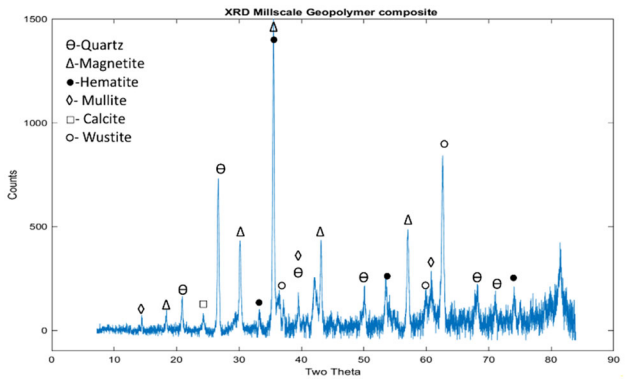

Fig. 5 XRD spectra for mill scale geopolymer composite. XRD signal shows peak positions for identified crystal structure. This composition showed the best results in terms of EMI SE

3.2 EMI shielding effectiveness

Figure 6 shows the geopolymer samples prepared for EMI SE testing according to ASTM-D4395 in the range from 0.1 to 1.5 GHz. Two types of samples were prepared: circular load samples and annular reference samples. The control sample were made from geopolymer, while all other samples have additives containing EMI shielding fillers. The gain (S) for load and references samples, each was recorded in decibel (dB) as $10 \times \log P_o/P_i$, where P_i and P_o were input and output power, respectively. The EMI SE was calculated as by subtracting the total

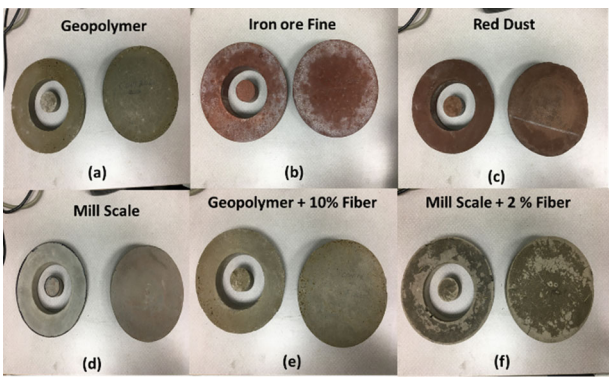

Fig. 6 The load (circular) and reference (annular) samples prepared for testing according to ASTM-D4395 standards

shielding measured with the load sample (S_{Load}) from the shielding measured with a reference specimen $S_{Reference}$ [30].

All the samples used here had a thickness of 30 mm. The S21 parameter of the reference and load samples were determined. The difference of reference and load gave us the EMI SE value in db. The surface of the samples was made smooth before taking the measurements. The surface of samples was made very flat to avoid any air gaps between the sample and the load cell. It has been observed that if there are air gaps while taking measurements, the S-parameter values might not be accurate [31].

Figure 7 shows the SE values calculated for the geopolymer and composites. Comparing the results to control (geopolymer), the iron ore fine and the red mud composites did not substantially change the EMI SE. The mill scale composites were found to have a positive impact on the SE; values changed from ~ 10 dB to (14–25 dB). To further improve the EMI SE, we added 2.3 wt% steel fibers (3–5 mm long, 200 μm diameter) and lowered the mill scale content to 38 wt% to accommodate steel fibers. As seen in Fig. 7e, significant improvement was found in SE over that obtained with mill scale composites; SE ranged between 28 and 69 dB. To isolate contribution of SS fiber, geopolymer composite with 10 wt% SS fiber was tested. Comparing Fig. 7e and f, the primary contribution to increasing the SE came from the addition of SS fibers. The increase in EMI SE due to mill scale and SS fibers can be attributed to either the increase in electrical conductivity or increase in magnetic property of the composites.

Since the electrical conductivity of geopolymer is low [32], we investigated the magnetic properties of the geopolymer composites, since EMI shielding effectiveness of a material can be attributed to its magnetic and electrical properties. As magnetic properties of materials play an important role in contribution to EMI SE, it is important to evaluate them. The electrical conductivity of geopolymer cementitious composites as well as mill scale shows very low electrical conductivity of the order of 10^{-6} S/cm [32]. Therefore, the observed EMI SE of the geopolymer composites has been ascribed to the inherent magnetic properties of the mill scale. In our experiments for measuring the magnetic properties, the mill scale geopolymer composites exhibited the maximum magnetization. The magnetic properties of the composites made using steel industry waste,

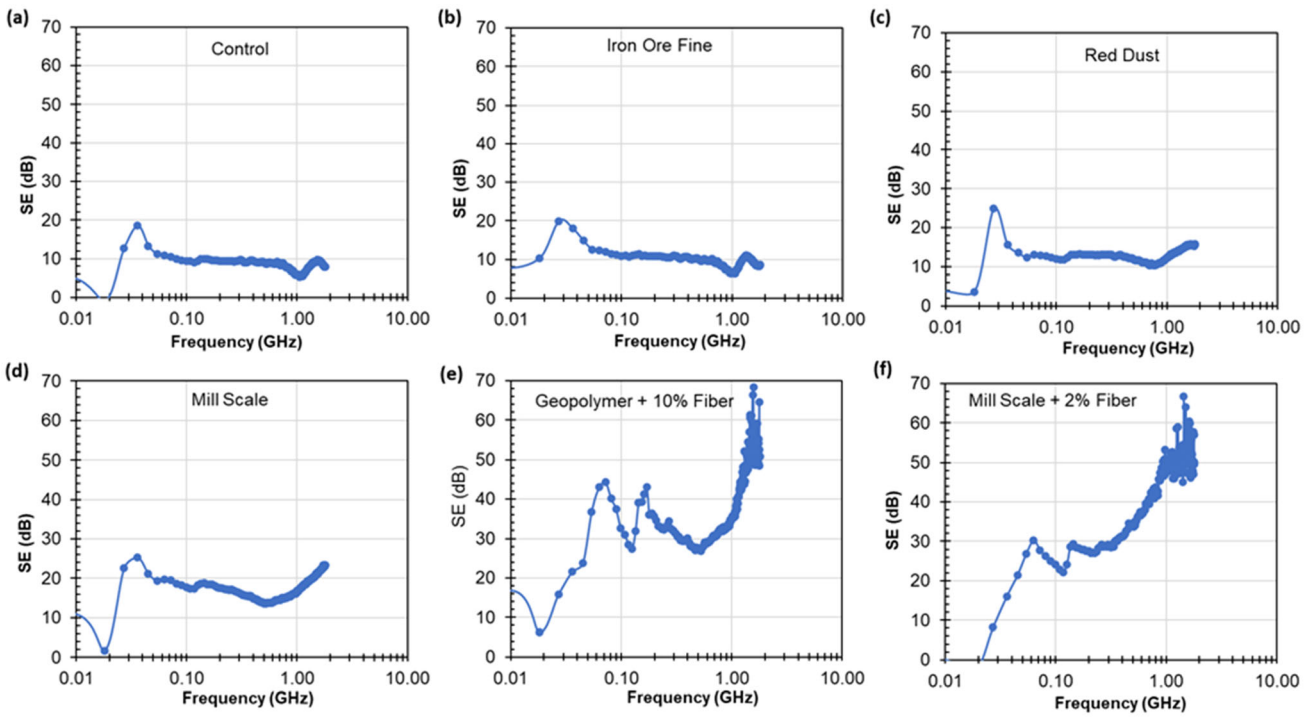

Fig. 7 The SE values in decibel (dB) obtained for geopolymer and composites according to ASTM-D4395 in the frequency range of 0.1–1.5 GHz

namely, iron ore fines, red dust, and mill scale geopolymer showed increased trend of magnetization characteristics. Based on these observations the contributions from electrical conductivity aspect are of little concern with respect to the observed shielding effectiveness of the developed composite. Hence mill scale geopolymer composite showed a high value for shielding effectiveness. The magnetic properties of geopolymer composites were studied using vibrating sample magnetometer. The Magnetization M (emu/g) vs magnetic field intensity in kilo Gauss (M–H curves) were plotted for the various geopolymer composites. The magnetic properties resulting from the study are given in the figure below. The detailed information results regarding the magnetic properties are included in Table 1 below.

From the graphs above the magnetic properties of various geopolymer composites were evaluated. It was found that the saturation magnetization of the control sample was the least 1.343 emu/g, while the saturation magnetization for the iron ore fine geopolymer sample was a bit higher at 1.761 emu/g. The EMI shielding effectiveness of any sample depends primarily on the electrical conductivity and magnetic property of the sample. The EMI shielding effectiveness values for the control and iron ore fine geopolymer samples were found to be the lowest; this can be attributed to the low values of saturation magnetization and electrical conductivity. Red dust showed saturation magnetization values of 10.691 emu/g much higher than the control and iron ore fine samples. The resulting EMI shielding effectiveness values for red dust geopolymer composites were up to 14 dB, while control and iron ore fines had EMI SE of 8–9 dB in the tested frequency range. The red dust geopolymer composite showed an improvement of 5–6 dB, compared to the control sample. This can be attributed to improved saturation magnetization. The mill scale geopolymer composites showed the maximum saturation magnetization of 22.16 emu/g, thus showing that the magnetic property of mill scale geopolymer played an important role in enhancing the EMI SE of the geopolymer composites. The improved EMI SE values of mill scale geopolymer can be attributed to its better magnetic properties as shown in Table 1, as the electrical conductivity of mill scale is poor due to the formation of oxides on the surface of iron, so the improved EMI SE values of mill scale geopolymer composites can be attributed to its magnetic properties. Magnetic material and their alloys have high saturation magnetization and good permeability [33]. Although their highly conductive behavior results in eddy current losses, leading to reduced permeability at lower frequencies. According to [33], the total shielding is a result of reflection SE and absorption SE. The reflection SE results in conductive materials and absorption mechanism results in materials which are magnetic in nature. The shielding effectiveness due to absorption is given by

$$SE_A = 8.7d\sqrt{f\pi\sigma\mu} \tag{2}$$

Here, mill scale possesses a high saturation magnetization of 22.165 emu/g and a high saturation magnetization results in high permeability, which could directly affect the EMI shielding effectiveness of the composite material. But due to eddy current losses the permeability reduces in lower frequency range, which could lead to reduced EMI SE in the lower frequency range. But in the higher frequency range the EMI SE is expected to show enhanced EMI SE values. This trend has been observed in mill scale geopolymer composites. As evident from Fig. 7d and f the EMI SE is less in the low-frequency range (MHz range) and higher in the high-frequency range (GHz range).

Thus, a high value of saturation magnetization results in higher EMI SE values particularly in the higher frequency range. Graphs in Fig. 8b show increased trend in EMI SE values as the saturation magnetization values increase.

Here, we demonstrate the use of mill scale and SS fiber to increase SE of geopolymer for the first time. The use of SS fibers in cementitious composites to

Table 1 Magnetic properties of various geopolymer composites obtained by performing experiments using a vibrating sample magnetometer model 880A, digital system measurements

Sample	Mass (g)	I_S (emu)	I_R (emu)	H_C (oe)	M_S (emu/g)	M_R (emu/g)
Control	0.2523	0.339	0.02535	97.1	1.343	0.1
Iron ore fine	0.2550	0.449	0.05476	138.5	1.761	0.214
Red dust	0.3458	3.699	0.18091	88.1	10.691	0.523
Mill scale	0.3842	8.516	0.49521	72.4	22.165	1.289

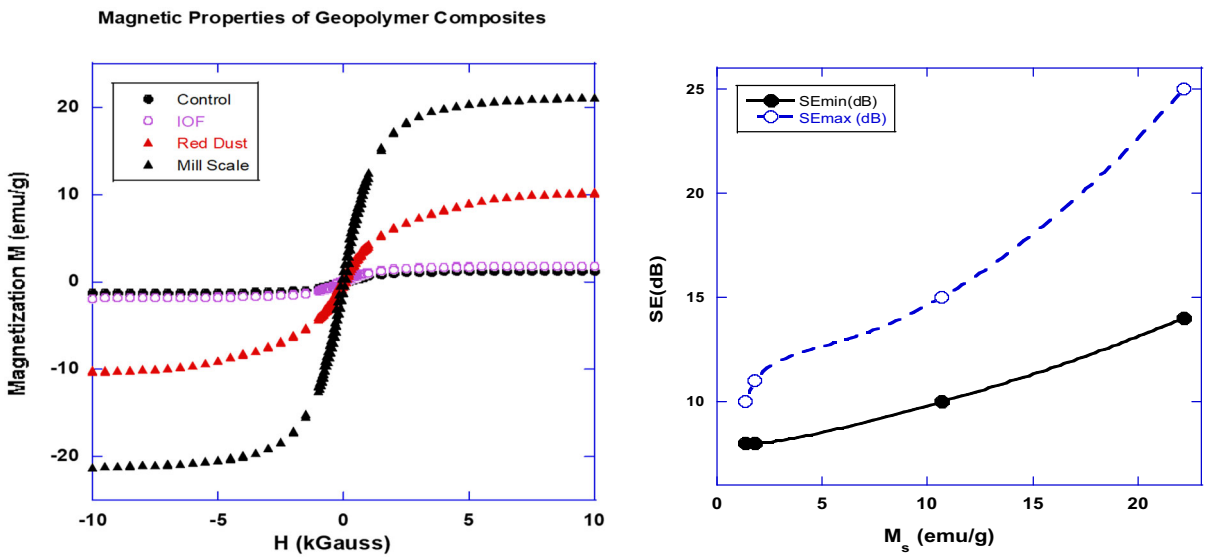

Fig. 8 **a** M–H curves for various geopolymer composites. **b** Shielding effectiveness vs saturation magnetization curve for various geopolymer composites corresponding to control, iron ore fine geopolymer, red dust geopolymer, and mill scale geopolymer sample

increase SE has been studied both experimentally and computationally. Ogunsola et al. have shown via simulations the increased EMI SE in the frequency range of 0–4 GHz for cementitious composites with steel fibers (0.5 mm diameter and 30 mm long), while the quantity of steel fibers in the concrete mix was assumed to not exceed 20–80 kg/m^3 [34]. Sun et al. have experimentally shown that reinforcing concrete with steel fibers (2–3% Volume fraction) improves the SE [35]. Yehia et al. showed that the conductivity and SE increases up to 50 dB in the frequency of 0.3 to 11 GHz which was reported for this composite mix due to the addition of straight steel fibers; however, the compressive strength remained unchanged [36]. This could be attributed to the known influence of SS fiber on the A.C. and D.C. conductivity of the composites [37].

3.3 Impedance spectroscopy of geopolymer composite

To examine the effect of steel waste and steel fiber additives on the A.C. impedance of geopolymer, impedance spectroscopy was performed between 100 Hz and 1 MHz. Nyquist data composing of real and imaginary impedance were obtained at varying frequencies as shown in Fig. 9. The real and imaginary impedance of most composites show logarithmic drop with frequency. The results of composites were compared to that of the geopolymer. In case of the mill scale composite, the real impedance between 30 Hz and 6 kHz was found to be higher compared to geopolymer and above 6 kHz it was found to be lower. Such a switching behavior was also seen in case of iron ore fine and red dust composites at 1.4 kHz and 500 Hz, respectively. However, the SS fiber composite showed almost similar real impedance as the pure geopolymer. The iron ore fine and red dust composites showed consistently lower imaginary impedance compared to pure geopolymer. The presence of zincite in red dust is responsible for observed lowest impedance in comparison to the iron ore fine and mill scale. In contrast, the mill scale composite showed consistently higher imaginary impedance until 500 kHz and at 1 MHz the imaginary impedance was found to be similar as that of pure geopolymer. A similar behavior was seen to happen at lower frequency in case of SS fiber composite, where the imaginary impedance was found to be consistently lower compared to pure geopolymer until 10 kHz and then at 500 kHz the imaginary impedance was found to be similar. The mill scale plus SS fiber composite showed an imaginary impedance switched at 500 Hz from being lower to being higher compared to pure geopolymer. To further understand the underlying electrical behavior, the data were modeled via equivalent circuit modeling.

In equivalent circuit modeling, several prior reported circuits were attempted to fit the data for all the composites. A circuit consisting of a resistor, a

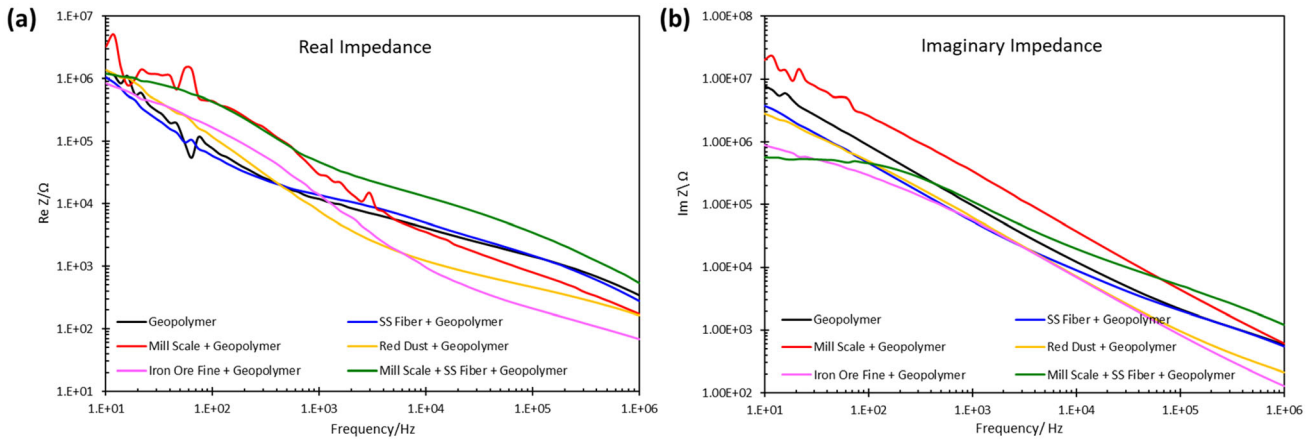

Fig. 9 **a** Real and **b** imaginary impedance for different geopolymer composites having different fillers

capacitor, and three R||C tanks as shown in Fig. 10a was able to best fit data from the six types of samples that were tested. The physical relevance of different R||C tanks corresponds to the different mechanisms of electrical charge transduction within the geopolymer or the composite, and the *R*1 and *C*1 values are believed to correspond to the nature of the electrode–composite or electrode–geopolymer contact interface. The best fit parameters along with their error are shown in Table 2. The resistance *R*2, *R*3, and *R*4 were found to be greater than *R*1 for all the cases. In case of pure geopolymer and SS fiber composite, the capacitance *C*1 was found best to be neglected. The R||C tanks were arranged in the order of decreasing value of *R*2 and the values of *R*2 and *C*2 are compared as shown in Fig. 10b and c. The value of *R*2 was found to be lower for the composite samples when compared to pure geopolymer samples, while red dust composite showed the lowest value for *R*2. This shows that lowest impedance to charge transport was observed in the red dust composite compared to pure geopolymer or other composites. The value of *R*2 for SS fiber composite was smaller than that for pure geopolymer; this shows that lower impedance to charge transport was observed in SS fiber composite. This could explain the better EMI SE values obtained with SS fiber composites when compared to pure geopolymer. This logic does not apply when comparing the value of *R*2 for SS fiber composite, which was found to be higher, when compared to that for red dust composite; the EMI SE of SS fiber composite was found to be much greater than that of the red dust composite. The same way, lower *R*2 value for mill scale and mill scale plus SS fiber composite compared to SS fiber composite was found inadequate to explain the higher EMI SE of the SS fiber composite.

In Fig. 7, the EMI SE value was found to be highest for SS fiber composite, followed by mill scale plus SS fiber composite, mill scale composite, and red dust composite; iron ore fine composite and geopolymer composite were found to show similar EMI SE values. The pattern for *R*2 value found in Fig. 10b does not agree with the pattern of EMI SE obtained in Fig. 7. For example, EMI SE was highest for SS fiber composite, but the value of *R*2 is not lowest for SS

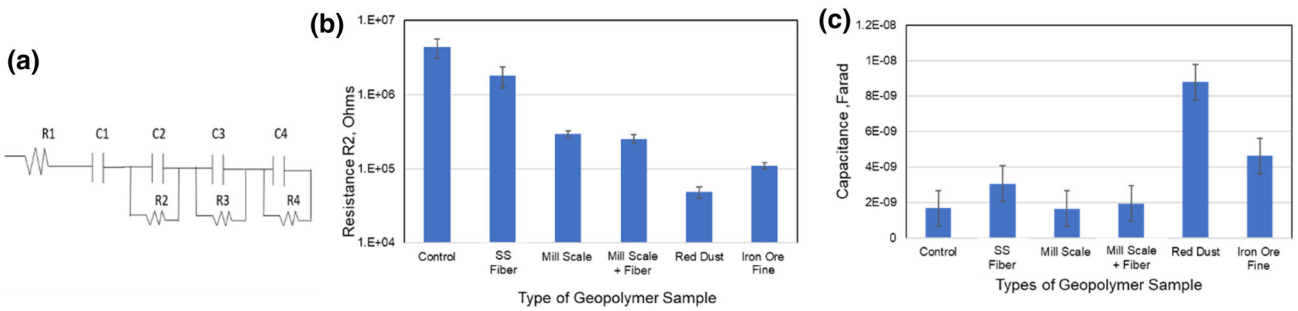

Fig. 10 Equivalent circuit modeling of impedance spectroscopy data for different geopolymer composites

Table 2 Resistive and capacitive parameter values obtained from the equivalent circuit modeling on impedance spectroscopy data for different geopolymer composites

	*R*1 (ohm)	*C*1 (Farad)	*R*2 (ohm)	*C*2 (Farad)	*R*3 (ohm)	*C*3 (Farad)	*R*4 (ohm)	*C*4 (Farad)
Control	238 ± 27	NA	4.4E6 ± 1.3E6	1.7E−9 ± 2.4E11	4.9E5 ± 4.4E2	2.4E−9 ± 1.8E−10	1.3E3 ± 0.7E2	1.7E−9 ± 2.4E-11
Red Dust	110 ± 8	3E−9 ± 9E−11	4.8E4 ± 8.2E3	8.8E−9 ± 6.2E−10	8.9E2 ± 0.9E2	6.8E−9 ± 5.4E−10	2.9E2 ± 0.1E2	1.3E−9 ± 8.3E−11
Iron Ore Fine	56 ± 4	6.3E−9 ± 3.7E−10	1.1E5 ± 1.1E4	4.6E−9 ± 1.8E−10	2.5E3 ± 4.4E2	9.5E−9 ± 7.2E−10	1.7E2 ± 0.1E2	3.4E−9 ± 2.35E−10
Mill Scale	121 ± 10	6.2E−10 ± 1.1E−11	2.9E5 ± 3.1E4	1.6E−9 ± 7.1E−11	3.5E3 ± 360.5	2.5E−9 ± 1.6E−10	5.8E2 ± 0.4E2	8.9E−10 ± 4.1E−11
Mill Scale + Fiber	427 ± 58	3.8E−9 ± 4.6E−10	2.5E5 ± 3.5E4	1.9E−9 ± 1.1E−10	1.5E4 ± 1.1E3	7.6E−10 ± 5.7E−11	3.7E3 ± 2.8E2	2.2E−11 ± 1.2E−11
SS Fiber	224 ± 29	NA	1.8E6 ± 5.5E5	3.1E−9 ± 6.8E−11	8.2E3 ± 6.1E2	2.2E−9 ± 1.5E−10	1.7E3 ± 1.1E2	4.5E−10 ± 2.4E−11

fiber composite. Similarly, in Fig. 10c, the value of $C2$ was found to be highest for red dust composite, followed by iron ore fine composite and mill scale composite; the value of $C2$ for pure geopolymer, SS fiber composite, and mill scale plus SS fiber composite were found to be similar and the lowest. The pattern in the value of $C2$ also does not agree with the pattern of EMI SE obtained in Fig. 7. This shows that electrical characteristics of the geopolymer and geopolymer composite justify the observed EMI SE. We hypothesize that the magnetic property of the composites must be responsible for the observed EMI shielding effectiveness in this study.

4 Conclusion

In summary, this study examined three wastes from steel industry, namely, mill scale, red dust, and iron ore fine as additives for making geopolymer-based EMI shielding composites. The presence of electrically conducting alkaline content of geopolymer helped in achieving EMI SE up to 10 dB in the frequency range 0.1 to 1.5 GHz. The addition of iron ore fine had the least change in EMI SE compared to control sample, while the addition of mill scale has shown the maximum enhancement in EMI SE up to 24 dB. Although the addition of 10 wt% fiber in the control showed EMI SE up to 69 dB. However, in the case of sample made using mill scale and steel fiber 2 wt% showed up to 67 dB and therefore it is possible to make geopolymer-based EMI shielding using mill scale which is an industrial waste and helps in saving an additional 8% of steel fiber and thus making it cost effective. Magnetic properties of geopolymer composites were also studied and was found that mill scale geopolymer had the highest saturation magnetization of 22.165 emu/g, followed by red dust geopolymer composite of 10.691 emu/g. The control and iron ore fine geopolymer samples showed the least saturation magnetization and the least EMI shielding effectiveness. Impedance spectroscopy and equivalent circuit modeling show that electrical conductivity alone was not responsible for the observed change in EMI SE upon addition of steel industry waste and SS fiber. The developed geopolymer-based shielding material to be used as building material the compressive strength of mill scale plus 2 wt% SS fiber has shown sufficient compressive strength of 22 MPa.

Acknowledgements

Availability of funds from NSF under Cooperative Agreement Number OIA1541079 (CFDA #47.083) through the Louisiana Experimental Program to Stimulate Competitive Research (EPSCoR) helped to conduct SEM analysis at the Institute for Micromanufacturing (IfM), one of the Core User Facilities (CUF) under the Charter of the Louisiana State-Wide Consortium for Innovation in Materials Manufacturing (CIMM).

Author contributions

RS, SA, and AR contributed to the study conception and design, material preparation, data collection, and analysis. WC aided in XRD and SEM studies. SA and JM contributed to mechanical testing. The first draft of the manuscript was written by RS and authors commented on the previous versions of the manuscript. All authors read and approved the final manuscript.

Funding

This work was supported by NSF under Cooperative Agreement Number OIA1541079 (CFDA #47.083) through the Louisiana Experimental Program to Stimulate Competitive Research (EPSCoR).

Data availability

The datasets generated during and/or analyzed during the current study are not publicly available due to competing financial interests but are available from the corresponding author upon reasonable request.

Declarations

Conflict of interests The authors declare financial interest and actively pursuing a US patent.

Ethical approval This article does not contain any studies on animals or human participant performed by any of the authors.

Supplementary Information: The online version contains supplementary material available at https://doi.org/10.1007/s10854-021-07674-9.

References

1. L. Hardell, M. Carlberg, Health risks from radiofrequency radiation, including 5G, should be assessed by experts with no conflicts of interest. Oncol. Lett. **20**(4), 15 (2020). https://doi.org/10.3892/ol.2020.11876
2. L. Hardell, R. Nyberg, [Comment] Appeals that matter or not on a moratorium on the deployment of the fifth generation, 5G, for microwave radiation. Mol. Clin. Oncol. (2020). https://doi.org/10.3892/mco.2020.1984
3. M. Bäckström, The threat from intentional EMI against the civil technical infrastructure. 16–19 (2006)
4. S. Zarei, M. Oryadi-Zanjani, N. Alighanbari, S.MJ. Mortazavi, Mother's exposure to electromagnetic fields before and during pregnancy is associated with risk of speech problems in offspring. J. Biomed. Phys. Eng. (2018). https://doi.org/10.31661/jbpe.v0i0.676
5. "No Title."
6. R.M. Novais et al., Pyrolysed cork-geopolymer composites: a novel and sustainable EMI shielding building material. Constr. Build. Mater. **229**, 116930 (2019). https://doi.org/10.1016/j.conbuildmat.2019.116930
7. M. Jung, Y. Lee, S.-G. Hong, J. Moon, Carbon nanotubes (CNTs) in ultra-high performance concrete (UHPC): dispersion, mechanical properties, and electromagnetic interference (EMI) shielding effectiveness (SE). Cem. Concr. Res. **131**, 106017 (2020). https://doi.org/10.1016/j.cemconres.2020.106017
8. A.P. Singh et al., Multiwalled carbon nanotube/cement composites with exceptional electromagnetic interference shielding properties. Carbon N. Y. **56**, 86–96 (2013). https://doi.org/10.1016/j.carbon.2012.12.081
9. W.L. Yao, G.X. Xiong, Y. Yang, Electromagnetic shielding effectiveness of nickel fiber-reinforced cement composites. Mater. Sci. Forum **898**, 2065–2070 (2017). https://doi.org/10.4028/www.scientific.net/MSF.898.2065
10. Y. Fan, L. Zhang, V. Volski, G.A.E. Vandenbosch, B. Blanpain, M. Guo, Utilization of stainless-steel furnace dust as an admixture for synthesis of cement-based electromagnetic interference shielding composites. Sci. Rep. **7**(1), 4–11 (2017). https://doi.org/10.1038/s41598-017-15779-7
11. S.W. Huang, X.S. Yi, G.H. Chen, M. Deng, M.S. Tang, Electromagnetic shielding effectiveness of cement based materials with scrap tires wire—FeCuNbSiB amorphous alloy powder. Adv. Mater. Res. **194–196**, 886–889 (2011). https://doi.org/10.4028/www.scientific.net/AMR.194-196.886
12. C. Tuan, L. Nguyen, Structural concrete mix for construction for electromagnetic wave/pulse shielding. U.S. Patent No. 9,681,592., (2017)
13. K. Neupane, D. Chalmers, P. Kidd, High-strength geopolymer concrete-properties, advantages and challenges. Adv. Mater. (2018). https://doi.org/10.11648/j.am.20180702.11
14. G. Bantsis, C. Sikalidis, M. Betsiou, T. Yioultsis, T. Xenos, Electromagnetic absorption, reflection and interference shielding in X-band frequency range of low cost ceramic building bricks and sandwich type ceramic tiles using mill scale waste as an admixture. Ceram. Int. **37**, 3535–3545 (2011). https://doi.org/10.1016/j.ceramint.2011.06.010
15. M. Ozturk, T. Depci, E. Bahceci, M. Karaaslan, O. Akgol, U.K. Sevim, Production of new electromagnetic wave shielder mortar using waste mill scales. Constr. Build. Mater. **242**, 118028 (2020). https://doi.org/10.1016/j.conbuildmat.2020.118028
16. Y. Fan, L. Zhang, V. Volski, G.A.E. Vandenbosch, B. Blanpain, M. Guo, Utilization of stainless-steel furnace dust as an admixture for synthesis of cement-based electromagnetic interference shielding composites. Sci. Rep. **7**(1), 15368 (2017). https://doi.org/10.1038/s41598-017-15779-7
17. Y.-J. Tan et al., Comparative study on solid and hollow glass microspheres for enhanced electromagnetic interference shielding in polydimethylsiloxane/multi-walled carbon nanotube composites. Compos. Part B Eng. **177**, 107378 (2019). https://doi.org/10.1016/j.compositesb.2019.107378
18. C.R. Ward, D. French, Determination of glass content and estimation of glass composition in fly ash using quantitative X-ray diffractometry. Fuel **85**(16), 2268–2277 (2006). https://doi.org/10.1016/j.fuel.2005.12.026
19. J.L. Jambor, J.E. Dutrizac, Occurrence and constitution of natural and synthetic ferrihydrite, a widespread iron oxyhydroxide. Chem. Rev. **98**(7), 2549–2586 (1998). https://doi.org/10.1021/cr970105t
20. V. Noval Lara, J. Carriazo, Fe3O4-TiO2 and Fe3O4-SiO2 core-shell powders synthesized from industrially processed magnetite (Fe3O4) microparticles. Mater. Res. (2019). https://doi.org/10.1590/1980-5373-mr-2018-0660
21. S.S. Amritphale, D. Mishra, M. Mudgal, R.K. Chouhan, N. Chandra, A novel green approach for making hybrid inorganic–organic geopolymeric cementitious material utilizing fly ash and rice husk. J. Environ. Chem. Eng. **4**(4), 3856–3865 (2016). https://doi.org/10.1016/j.jece.2016.08.015
22. Z. Wang et al., The desirable dielectric properties and high thermal conductivity of epoxy composites with the cobweb-structured SiCnw–SiO2–NH2 hybrids. J. Mater. Sci. Mater.

Electron. **32**(16), 20973–20984 (2021). https://doi.org/10.1007/s10854-021-06543-9

23. S. Patra, A. Pattanaik, A.S. Venkatesh, R. Venugopal, Mineralogical and chemical characterization of low grade iron ore fines from barsua area, eastern india with implications on beneficiation and waste utilization. J. Geol. Soc. India **93**(4), 443–454 (2019). https://doi.org/10.1007/s12594-019-1199-4
24. M. Alkan, M. Bugdayci, A. Turan, F. Demirci, and O. Yucel, A comparative study on the reduction of mill scale from continuous casting processes. 2014.
25. T. Hou et al., Hierarchical composite of biomass derived magnetic carbon framework and phytic acid doped polyanilne with prominent electromagnetic wave absorption capacity. J. Mater. Sci. Technol. **68**, 61–69 (2021). https://doi.org/10.1016/j.jmst.2020.06.046
26. J. Liu et al., Self-assembled MoS2/magnetic ferrite CuFe2O4 nanocomposite for high-efficiency microwave absorption. Chem. Eng. J. **429**, 132253 (2022). https://doi.org/10.1016/j.cej.2021.132253
27. C.M. Vieira, R. Sanchez Rodriguez, S. Monteiro, N. Lalla, N. Quaranta, Recycling of electric arc furnace dust into red ceramic. J. Mater. Res. Technol. (2013). https://doi.org/10.1016/j.jmrt.2012.09.001
28. T. Sofilić, V. Novosel-Radovi, S. Cerjan-Stefanovic, A. Rastovcan-Mioc, The mineralogical composition of dust from an electric arc furnace. Mater. Tehnol. **39**, 149–154 (2005)
29. J. Wang et al., Construction of 1D heterostructure NiCo@C/ZnO nanorod with enhanced microwave absorption. Nano-Micro Lett. **13**(1), 175 (2021). https://doi.org/10.1007/s40820-021-00704-5
30. R. Valente, C. De Ruijter, D. Vlasveld, S. Van Der Zwaag, P. Groen, Setup for EMI shielding effectiveness tests of electrically conductive polymer composites at frequencies up to 3.0 GHz. IEEE Access **5**, 16665–16675 (2017). https://doi.org/10.1109/ACCESS.2017.2741527
31. T. Letertre, P. Pouliguen, P. Sabouroux, Electromagnetic characteristics measurement setup at variable temperatures using a coaxial cell. Adv. Mater. Sci. Eng. **2019**, 3646979 (2019). https://doi.org/10.1155/2019/3646979
32. S. Hanjitsuwan, P. Chindaprasirt, K. Pimraksa, Electrical conductivity and dielectric property of fly ash geopolymer pastes. Int. J. Miner. Metall. Mater. **18**(1), 94–99 (2011). https://doi.org/10.1007/s12613-011-0406-0
33. V. Shukla, Review of electromagnetic interference shielding materials fabricated by iron ingredients. Nanoscale Adv. **1**(5), 1640–1671 (2019). https://doi.org/10.1039/C9NA00108E
34. A. Ogunsola, U. Reggiani, and L. Sandrolini, Shielding properties of conductive concrete against transient electromagnetic disturbances, In 2009 IEEE International Conference on Microwaves, Communications, Antennas and Electronics Systems. pp. 1–5, (2009). https://doi.org/10.1109/COMCAS.2009.5385975.
35. X. Zhang, W. Sun, Electromagnetic shielding and absorption properties of fiber reinforced cementitious composites. J. Wuhan Univ. Technol. Sci. Ed. **27**(1), 172–176 (2012). https://doi.org/10.1007/s11595-012-0430-6
36. S. Yehia, N. Qaddoumi, M. Hassan, B. Swaked, Conductive concrete for electromagnetic shielding applications. Adv. Civ. Eng. Mater. **3**(1), 270–290 (2014). https://doi.org/10.1520/ACEM20130107
37. J. Douglas, E.J. Garboczi, Intrinsic viscosity and polarizability of particles having a wide range of shapes. Adv. Chem. Phys. **91**, 85–153 (2007)